Commun. Comput. Phys.
doi: 10.4208/cicp.391011.260112s

Vol. **13**, No. 3, pp. 900-915
March 2013

Molecular Dynamics Simulations of Nanoparticle Interactions with a Planar Wall: Does Shape Matter?

Andreas Fuchs[1,*], David Kauzlarić[2], Andreas Greiner[1], Sauro Succi[2,3] and Jan. G. Korvink[1,2]

[1] *Laboratory for Simulation, Department of Microsystems Engineering (IMTEK), University of Freiburg, Georges-Köhler-Allee 103, 79110 Freiburg, Germany.*
[2] *School of Soft Matter Research, Freiburg Institute for Advanced Studies, University of Freiburg, Albertstr. 19, 79104 Freiburg, Germany.*
[3] *Istituto Applicazioni Calcolo, CNR, via dei Taurini 9, 00185, Roma, Italy.*

Received 31 October 2011; Accepted (in revised version) 26 January 2012

Available online 29 August 2012

Abstract. We investigate the hydrodynamic interactions of spherical colloidal nano particles and nano tetrahedra near a planar wall by means of molecular dynamics (MD) simulations of rigid particles within an all-atom solvent. For both spherical and nano-tetrahedral particles, we find that the parallel and perpendicular components of the local diffusion coefficient and viscosity, show good agreement with hydrodynamic theory of Faxén and Brenner. This provides further evidence that low perturbations from sphericality of a nanoparticle's shape has little influence on its local diffusive behaviour, and that for this particular case, the continuum theory fluid dynamics is valid even down to molecular scales.

PACS: 47.85.Dh, 47.11.Mn, 82.70.Dd

Key words: Molecular dynamics simulation, nanoparticle, hydrodynamic interaction.

1 Introduction

The diffusion of suspended particles in liquids is one of the most fundamental transport processes in physical chemistry, with many applications in material science, chemical engineering, and biology. Indeed, such diffusion processes may significantly affect the properties of the liquid suspension; for instance, it is known that particle diffusion sets the rate-limiting step to many chemical reactions in liquids [1], and that the addition of

*Corresponding author. *Email addresses:* fuchs@speag.com (A. Fuchs), david.kauzlaric@frias.uni-freiburg.de (D. Kauzlarić), andreas.greiner@imtek.uni-freiburg.de (A. Greiner), succi@iac.cnr.it (S. Succi), jan.korvink@imtek.uni-freiburg.de (J. G. Korvink)

particles to liquids leads to an increase of the viscosity, as predicted by Einstein nearly a century ago [2]. The diffusion of a suspended particle within a liquid is inversely related to the dynamic viscosity of the liquid, according to the Fluctuation-Dissipation-Theorem (FDT) [3], as combined with Stoke's law for the drag experienced by a colloidal particle within a fluid solvent [4]. The mathematical expressions associated with these two conceptual pillars are typically derived in free-space, where long-range hydrodynamic correlations can develop without hindrance. However, in the presence of solid walls (confined flows), or other colloidal particles (dense suspensions), it is known that both particle diffusivity and liquid viscosity acquire significant corrections, due to the distortions experienced by hydrodynamic correlations as compared to the ideal case of a single particle within an infinite fluid domain. Such finite-size and finite-concentration effects are paramount to most practical applications, typically involving colloidal suspensions of nano-particles of assorted shapes [5, 6]. In this paper, we shall focus on finite-size effects in confined nanofluids. Several experimental [7–11] as well as theoretical [12] studies have focussed on these effects for colloidal particles. More specifically, we compute the local diffusion coefficients of a suspended nanoparticle as a function of its distance from a planar wall, along both parallel and perpendicular directions to the wall. To this purpose, extensive molecular dynamics (MD) simulations are performed, and compared against the analytical results, as provided by Faxén's and Brenner's continuum hydrodynamics theories [13–15]. Two basic shapes are explored, spherical and tetrahedral, the latter being of special interest to the growth of optical crystals through self-assembly of silicon nano-particles [16, 17].

Deviations from continuum hydrodynamics in the vicinity of the wall have made the object of basic molecular dynamics investigations in the past. Vergeles et al. performed molecular dynamics simulations of a single sphere approaching a planar wall at constant velocity u [18]. These authors confirmed the validity of hydrodynamics sufficiently away from the wall, and showed that the near-wall divergence disappears in the atomistic treatment due to a depletion of the fluid layer. More recently, Challa and van Swol [19], alluded to the importance of solvation forces, namely the conservative forces experienced by the sphere independently of its speed.

Since we aim at a realistic model of a nanoparticle immersed in a liquid and ask for the validity of Faxén's and Brenner's hydrodynamic theories in this case, our simulation setup will differ from the one used in the aforementioned works in several aspects. i) Instead of assigning a constant velocity to the nanoparticle, requiring the assumption that its mass is infinite, we track its thermal equilibrium fluctuating motion and apply statistical mechanical theory (Green-Kubo relations) and the Stokes-Einstein relation to compute transport coefficients from velocity autocorrelation functions (VACFs). ii) As a consequence, our nanoparticle is not just small in terms of length scales, but in addition, it will not have infinite mass. On the other hand, we aim at approximately Brownian behaviour, i.e. an exponentially decaying VACF. For this, we require a mass density for the nanoparticle which is considerably larger than the fluid density. It will turn out that Brownian behaviour is already sufficiently achieved for a mass density ratio of 10. iii) Investigating

thermal equilibrium also means that we consider the case of vanishing Reynolds number $Re \to 0$, in contrast to the intermediate Reynolds numbers $Re = 0.01, \cdots, 0.3$ in [19] and, for the nanoscale, very high Reynolds numbers $Re = \mathcal{O}(1)$ in [18]. iv). We do not monitor net forces on the particle, but velocity fluctuations applied to the Green-Kubo definition of the diffusivity, thus there is no need to split into static (conservative, solvation) and dynamic (drag, lubrication) force contributions [19]. v) Vergeles et al. and Challa et al. mostly focus on non-molecular ideally smooth walls and spheres. We believe that we should focus on walls and spheres with molecular structure, which, e.g., reduces the depletion of fluid layers near walls [18].

The advantage of our approach is that thermal equilibrium fluctuations provide all admissible motions of the nanoscale object. This allows the investigation of the motion parallel and perpendicular to the wall within one and the same simulation. Hence we can compare to both Faxén's and Brenner's theories. One drawback of our approach is that the additional fluctuations of the nanoparticle and the molecular structure make the computed transport coefficients more noisy, increasing the size of the error bars.

Our investigations show that for both shapes, the MD results are in agreement with Faxén's and Brenner's theories, for parallel and perpendicular diffusion, respectively. This applies to a large range of distances from the wall, down to one molecular radius, where the validity of continuum hydrodynamics is questionable, showing a nonphysical singularity of the perpendicular diffusivity at zero distance. Our results show that, firstly, for the specific phenomenon in point, we find that continuum hydrodynamics holds down to the molecular scale. Secondly, the diffusivity shows no shape-dependence, i.e. tetrahedron and sphere show equivalent results in line with the statistical precision. The latter statement, though, is likely to be challenged when using anisotropic tetrahedra or ellipsoids.

The paper is organized as follows. In Section 2 we discuss the hydrodynamic correction terms for the drag force experienced by particles close to walls and also present the main statistical mechanical tools required for the analysis of the MD simulations. We then present our simulation method and setup in Section 3 and, finally, in Section 4 we present and discuss the numerical results.

2 Theoretical background

The drag force $\mathbf{F}_d$ on a rigid sphere with radius R, moving with a constant relative velocity $\mathbf{v}$ through a viscous fluid with shear viscosity η, is given by Stokes' law. For the derivation of Stokes' law we assume laminar flow ($\mathrm{Re} \ll 1$), in which case the Navier-Stokes equation reduces to the following static balance between pressure drive and dissipation [4]:

$$\nabla p = \eta \Delta \mathbf{v}. \tag{2.1}$$

This can be solved for the pressure p along the velocity component u given in spherical coordinates r and Θ, where $\Theta = 0$ and $\Theta = \pi$ denote the front and rear side of the sphere,

respectively:

$$p(\Theta, r=R) = p_0 + \frac{3\eta u}{2R}\cos\Theta, \tag{2.2}$$

where p_0 is the bulk pressure.

By integrating the pressure field over the surface of the sphere, the drag force F_d along u takes the familiar form of Stokes's law:

$$F_d = 6\pi\eta R u. \tag{2.3}$$

The above relation holds in free space. Once the sphere is brought in the vicinity of a planar wall, the drag force F_d shows a significant, anisotropic, increase, due to the hydrodynamic pressure caused by the interaction of the sphere with the planar wall. For the case of the perpendicular diffusion, this enhancement develops into a formal singularity in the limit of zero distance from the wall. The particle then experiences a local viscosity that depends on the distance to the wall and on the direction of motion, i.e. parallel versus perpendicular.

The analytical description of the viscosity increase in the parallel direction was first developed by Faxén in 1922 [13,15], who introduced a correction term, $\lambda^{\parallel}$, accounting for the corrections to the Stokes' law. The perpendicular correction term, $\lambda^{\perp}$, was analytically derived by Brenner with the method of reflections [14, 15]. The corresponding extended Stokes' law reads as follows:

$$F_d^{\parallel,\perp} = 6\pi\eta R u^{\parallel,\perp}\cdot\lambda^{\parallel,\perp}, \tag{2.4}$$

$$\lambda^{\parallel} = \left(1 - 9/16 d^{-1} + 1/8 d^{-3} - 45/256 d^{-4} - 1/16 d^{-5}\right)^{-1}, \tag{2.5}$$

$$\lambda^{\perp} = \frac{4}{3}\sinh\alpha \sum_{n=1}^{\infty} \frac{n(n+1)}{(2n-1)(2n+3)} \left[\frac{2\sinh(2n+1)\alpha + (2n+1)\sinh 2\alpha}{4\sinh^2(n+1/2)\alpha - (2n+1)^2\sinh^2\alpha} - 1\right], \tag{2.6}$$

where $d = 1 + z/R$ is the distance of the sphere's centre of mass to the wall normalised to the sphere's effective radius R, z is the distance of the sphere's effective surface to the wall, and $\alpha = \cosh^{-1} d$. It can be checked that the above expression for $\lambda^{\perp}$ tends to 1 in the limit $z/R \to \infty$ (bulk) and to R/z in the opposite limit $z/R \to 0$ ($d \to 1$), yielding a formal singularity at vanishing distance from the wall.

A closely related view on the problem of wall effects is Felderhof's [20]. He derived theoretically a qualitative change of the hydrodynamic tail of the nanoparticle's velocity autocorrelation function from $t^{-3/2}$ to $t^{-5/2}$. This result was obtained from a first order approximation in R/z and, concerning the dependence of the particle's mobility on z, is equivalent to Lorentz' findings [15, 21] which are only reliable for small R/z, whereas Brenner's and Faxén's theories represent the generalisation to arbitrary relative distances. Reducing, e.g., Faxén's equation (2.5) to Lorentz' result means to truncate after the term proportional to d^{-1}. This makes Brenner's and Faxén's theories more useful in

the present context, since we are especially interested in the behaviour of nanoparticles at distances z for which $R/z \gtrsim 1$. On the other hand in contrast to Brenner's and Faxén's theories, Felderhof's general approach is not limited to the low frequency Stokes regime (treated in this work) and can be used as a starting point for the analysis of, e.g., the neutrally buoyant case, which is only briefly mentioned in Section 4.1 of the present paper. Also note the work by Pagonabarraga et al. [22], which describes the solvent by a Lattice-Boltzmann method and provides long time power law decays of both the velocity correlation and angular velocity correlation functions of a colloidal particle near a wall.

The effective radius R and the normalised distance to the wall $d-1=z/R$ require a definition as soon as molecular interactions are introduced [18, 19]. Since all elements of our simulated systems, i.e., the fluid, the immersed particle, and walls will be constructed from point-particles with the same particle density n and interacting with the same Lennard Jones (LJ) potential, our definitions are based on the approach to assign effective volumes to all these particles. Following this argument, we get $R=R'+\bar{d}_A/2$ where R' is the distance of the nanoparticle's centre of mass to the coordinate of the farthest LJ particle it contains, and $\bar{d}_A \approx n^{-1/3}$ is the average distance between LJ particles. As a consequence, the nanoparticle's normalised distance to the wall is

$$d-1=\frac{z}{R}=\frac{d'-R'-\bar{d}_A}{R}=\frac{d'-\bar{d}_A/2}{R}-1, \tag{2.7}$$

where d' is the distance between the nanoparticle's centre of mass and the coordinate of the "innermost" layer of LJ particles forming the wall. Note that this definition is different from the definition in [18, 19], where fluid particles were treated as point particles in the definition of an effective radius and distance, and it was assumed, e.g. that the "free space" between a fluid particle and the spherical surface where the LJ potential diverges entirely belongs to the sphere.

We express the hydrodynamic transport coefficient η in terms of the microscopic molecular dynamics (MD) variables by the Green-Kubo and Stokes-Einstein relations, investigating whether the hydrodynamic corrections based on continuum hydrodynamics also hold for the case of our nanoparticles, just a few nanometres in diameter.

In the limit of low Reynolds numbers we can combine the equations of Brownian motion with the drag force from Stokes' law and obtain the Stokes-Einstein relation that relates the diffusion coefficient to the viscosity of the fluid [23]

$$D=\frac{k_B T}{6\pi\eta R}\,, \tag{2.8}$$

with D the diffusion coefficient, k_B the Boltzmann constant, T the temperature. We will use this relation to replace the calculation of the distance dependent viscosity by computing the diffusion coefficients. The anisotropic increase of the viscosity is analytically described by the correction terms (2.5) and (2.6). Thus we assume that we can calculate the viscosity profile from the reciprocal diffusion profile.

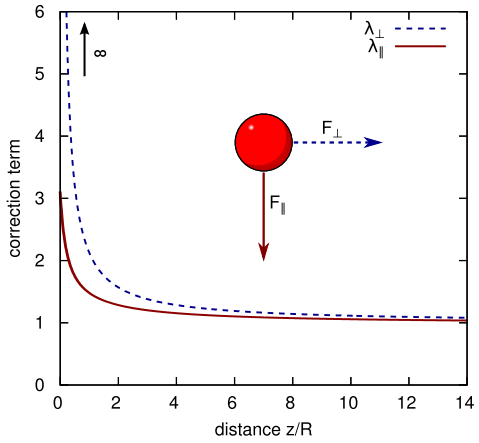

Figure 1: The analytical solution of the anisotropic increase of the drag force on a spherical object moving relative to a planar wall according to Faxén's (2.5) and Brenner's (2.6) correction terms for Stoke's law.

The diffusion coefficient will be computed from the Green-Kubo integral of the velocity auto-correlation function of the nanoparticle's centre of mass

$$D = \int_0^\infty \langle v(\tau)\, v(0)\rangle \, \mathrm{d}\tau, \tag{2.9}$$

where the bracket indicates time averaging and also ensemble averaging over several MD realizations, and v stands for one of the velocity components. Since we measure diffusion constants $D_{||}$ parallel and $D_\perp$ perpendicular to the wall, we use the perpendicular velocity component for $D_\perp$ and average over the two parallel components for $D_{||}$.

3 Simulation method and setup

3.1 Molecular fluid dynamics

We perform three-dimensional molecular dynamics (MD) simulations, with about 6.7×10^4 solvent molecules over a time span of about 10 million timesteps. Macroscopic quantities, such as the particle diffusivity, are computed by taking statistical averages over micro canonical ensembles provided by the MD simulations.

We use the Velocity Verlet integrator to compute the trajectory of the fluid particles.

The Lennard-Jones (LJ) (12,6) potential

$$V_{LJ}(r_{ij}) = 4\epsilon\left[\left(\frac{\sigma}{r_{ij}}\right)^{12} - \left(\frac{\sigma}{r_{ij}}\right)^{6}\right] \tag{3.1}$$

is used to model the interaction forces, where $r_{ij} = |\mathbf{r}_i - \mathbf{r}_j|$ is the distance between atoms i and j, ϵ is the depth of the potential well and σ is the distance at which the inter-particle potential is zero.

We truncate the tail of the LJ potential at its minimum at $r_c = 2^{1/6}\sigma$ and shift the minimum to zero. Hence, we treat only the repulsive part of the potential, to obtain the so-called Weeks-Chandler-Anderson (WCA) potential, [24]

$$V(r) = \begin{cases} V_{LJ}(r) - V_{LJ}(r_c), & \text{for } r \leq r_c, \\ 0, & \text{for } r > r_c, \end{cases} \tag{3.2}$$

which we use for all simulations throughout this paper. Despite its simplicity, this potential proves adequate for the inspection of hydrodynamic effects in molecular fluids [23,25,26].

3.2 The nanoparticle: rigid body dynamics

To keep the model as close as possible to the assumptions of Faxén and Brenner [13,15], we model the nanoparticle as a rigid-body (RB). In a particle-based RB the positions of a number of particles, shaping the RB, are strictly fixed to the local coordinate system centred in the RB's centre of mass. This way, only three translational degrees of freedom (DOFs) X,Y,Z and three rotational DOFs θ,ψ,ϕ, have to be tracked. Forces are computed between the fluid particles and the body's particles and for simplicity, the same interaction potential (3.1) as inside the fluid is used. No forces are computed between the body's particles, as their position in the coordinate system of the centre of mass is fixed. Forces acting between the fluid particles and the body particles are split into linear force and torque, with respect to the centre of mass. Because of d'Alembert's principle, the linear forces and torques of the body's particles can be accumulated. The resulting linear force and torque are applied only to the 6 DOFs X,Y,Z,θ,ψ,ϕ. The update of these 6 DOFs according to the force and torque defines a translation and rotation of the RB's local coordinate system and hence of the RB-particles fixed in it.

To compute the orientation of the nanoparticle we use *quaternions* as combined with a Verlet-like time integration scheme, developed by Omelyan [27].

3.3 Simulation setup

The physical units of our LJ-model system depend on the material to be represented. As a simple approximation the LJ-potential is used for many fluids, although in a strict sense, it only represents accurately noble gases, such as Argon. For the latter, the values for σ and ϵ are given in Table 1. In these units, the diameter of the spherical nanoparticle is 2.5 nm, hence very small.

Using MD, we simulate a colloidal nanoparticle performing Brownian motion. We make use of several equilibrium MD simulations of one nanoparticle in a LJ fluid and at different initial distances to a planar wall. We track the position and the velocity of the diffusing nanoparticle and compute the velocity-autocorrelation-function (VACF) of the nanoparticle's velocity. With the Green-Kubo expression (2.9), we compute the diffusion

Table 1: The molecular dynamics (MD)-units and their values for Argon in SI-units.

parameter	MD-unit	values for argon [SI-units]
length	$l^* = \sigma_{LJ}$	3.40×10^{-10} m
energy	$\epsilon^* = \epsilon_{LJ} = k_B T$	1.66×10^{-21} J
mass	$m^* = m_{LJ}$	6.69×10^{-26} kg
time	$t^* = \sigma_{LJ}\sqrt{m^*/\epsilon^*}$	2.16×10^{-12} s

coefficient. Our goal is to obtain a profile of the parallel and perpendicular components of the diffusion coefficient as a function of the nanoparticle's distance from the planar wall. Since the nanoparticle is unconstrained and allowed to perform free Brownian motion in the entire simulation domain we can not simply associate the diffusion coefficients that we measure for a nanoparticle, to its initial or average position. Therefore, we apply a sorting algorithm that uses the instantaneous position of the nanoparticle to generate pieces of the velocity trajectory that belong to different layers, corresponding to ranges of distances of the nanoparticle to the planar wall (cf. Fig. 2). Differently to the simplified figure, these ranges may overlap and vary in width from $\sim 3\sigma$ close to the wall to $\sim 7\sigma$ more in the bulk. Besides the overlap, no additional smoothing of the data points is performed. We then compute the VACF for each of these pieces of the velocity trajectory, and compute a weighted average of all VACFs belonging to the same layer. We finally use the Green-Kubo relation to obtain the diffusion coefficients from the averaged VACF and associate this coefficient with the average particle position of all trajectories of a layer.

Table 2 summarises the parameters that are used for all simulations. We use periodic boundary conditions in all directions with the lateral sizes of the domain given in the table. To model the planar wall with normal vector in z-direction (the particle layer on the left in Fig. 2), we freeze a layer of fluid particles, initially arranged in a face-centred cubic (FCC) lattice and exclude these particles from the time integration. Due to the periodicity of the simulation domain, there is in fact a periodic array of walls in z-direction. The wall thickness is one FCC elementary cell length a_c (cf. Table 2), and hence larger than the cutoff r_c. By choosing the largest domain size in z-direction, we try to minimise finite size-effects, although we cannot exclude them completely.

We run 40 and 35 simulations with different initial conditions for the sphere and the tetrahedron, respectively. Besides the initial velocities of the fluid particles, the initial conditions differ in the nanoparticle's initial distance to the wall. Each of the simulations consists of 2×10^7 production timesteps following 10^5 thermalisation and equilibration timesteps. Thermalisation is performed by a rescaling of the velocities of the fluid particles periodically at specific time steps and subsequent relaxation periods. The nanoparticle's degrees of freedom are not rescaled but converge to the desired temperature along with the fluid particles. The fluid's and the nanoparticle's average temperatures during the production run are both always within 2% of the desired value.

During the random walk, the nanoparticle usually travels through the complete simulation volume. Hence, it is not necessary to position the nanoparticle of the ensemble

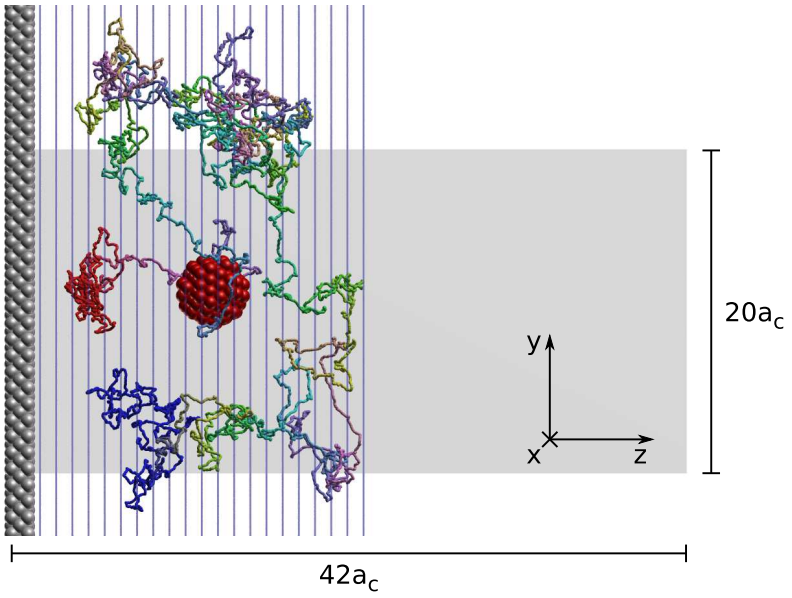

Figure 2: Illustration of the subdivision of the simulation volume into layers parallel to the wall for computing local velocity-autocorrelation-functions (VACF) and diffusion constants. The unit of length used in the figure is $a_c \approx 1.79\sigma$ (cf. Table 2) and is used to denote the dimensions of the simulation box. The colour-coding of the representative particle trajectory indicates its start (red) and end (blue). For a better visualisation, the trajectory extends to the neighbouring periodic boxes instead of being cut and shifted back to the original simulation box shown in light grey.

simulations at even greater distances to the wall. The most interesting region with respect to the correction terms, is the one close to the wall (cf. Fig. 1), which is also the statistically best covered one.

We simulate spherical nanoparticles consisting of 140 MD particles and nano tetrahedra of 56 MD particles. To construct the nanosphere, we initially place particles in a FCC lattice and select those inside a spherical volume with radius R'. This radius is used as starting point to compute the effective hydrodynamic radius $R \approx 3.69\sigma$ (cf. Table 2) as described in Section 2.

For the nano-tetrahedron, we additionally cut the particles inside the spherical volume by four planes corresponding to the faces of the tetrahedron. Here, we use an effective radius of $R \approx 2.60\sigma$. To obtain the effective radius for the tetrahedron, we first inflate the tetrahedron along its surface normals by $\bar{d}_A/2$ and then calculate the radius for a sphere with the same surface area. This choice is motivated by the fact that hydrodynamic interactions act through the nanoparticle's surface. Interestingly, computing the effective radius from D as obtained with Green-Kubo of a periodic bulk simulation and the known viscosity of the LJ-fluid, leads to a very similar result for the effective radius R. In order to ensure Brownian motion the mass density of the nanoparticles is set to $10\rho_0$ where ρ_0 is the density chosen for the LJ-fluid. This is realised by setting the mass of a single rigid body particle to $m_{\mathrm{RB}} = 10m_f$ where m_f is the mass of a fluid particle.

Table 2: The basic setup of the nanoparticle molecular dynamics (MD)-simulations.

parameter	value: MD-units	for Argon
FCC cell constant a_c	1.79	0.61 nm
simulation domain	$20\times20\times42a_c^3$	3.77×10^3 nm^3
number of particles	67200	–
density n	0.7	1.70×10^3 kg m^{-3}
temperature T	1.0	120 K
timestep	0.003	8.64×10^{-15} s
equilibration time	$10^5\Delta t$	8.64×10^{-10} s
simulation time	$2\cdot10^7\Delta t$	1.73×10^{-7} s
number of simulations (sphere/tetrahedron)	40/35	–
cut-off range r_c	$2^{(1/6)}$	0.38 nm
effective particle radius (sphere/tetrahedron) R	3.69/2.60	1.25/0.89 nm
mass of sphere M_s	140×10	9.37×10^{-23} kg
mass of tetrahedron M_t	56×10	3.75×10^{-23} kg

4 Results

4.1 Brownian motion

First, we verify in a periodic bulk liquid that our choice for the nanoparticle mass, or, more specifically, the ratio of nanoparticle to fluid mass densities $\rho_{\mathrm{RB}}/\rho_{\mathrm{f}}=10$ allows us to assume Brownian behaviour and hence the Stokes-Einstein relation in its simple form (2.8). This is the case, if the nanoparticle's velocity autocorrelation function (VACF) decays exponentially. Note that this strict definition of Brownian motion is not consistently used in the literature. More general definitions including non-exponential VACFs can be found as well (cf., e.g., [20]). Fig. 3 shows the VACFs exemplarily for the sphere, on the left for $\rho_{\mathrm{RB}}/\rho_{\mathrm{f}}=1$, and on the right for $\rho_{\mathrm{RB}}/\rho_{\mathrm{f}}=10$. We used the same timestep of $\Delta t=1.152\times10^{-14}$s for the light and the heavy nanoparticle simulations, since the accelerations of the light fluid particles are the limiting factor for Δt. While the VACF for equal mass densities shows an approximately double exponential behaviour, the increased nanoparticle mass density leads to a VACF that can be sufficiently well fitted by a single exponential representing an extended region II as compared to $\rho_{RB}/\rho_f=1$. By doing so the largest error of $\approx$20% can be observed for the exponential's extrapolated value at $t=0$ which was not constrained to $3k_BT/M$ during fitting. This error stems from disregarding region I. Note that hydrodynamic theory predicts in the incompressible case that the VACF decays approximately exponentially in region II with an extrapolated value at $t=0$ of $\approx 3k_BT/(M+M_f/2)$, where M_f is the fluid mass displaced by the particle due to vortex diffusion (for details cf., e.g., [4, 28]). This effect represented by region I is clearly dominant for $\rho_{RB}/\rho_f=1$ and strongly reduced for $\rho_{RB}/\rho_f=10$. Note further, that increasing the mass density ratio increases the characteristic time for Brownian motion

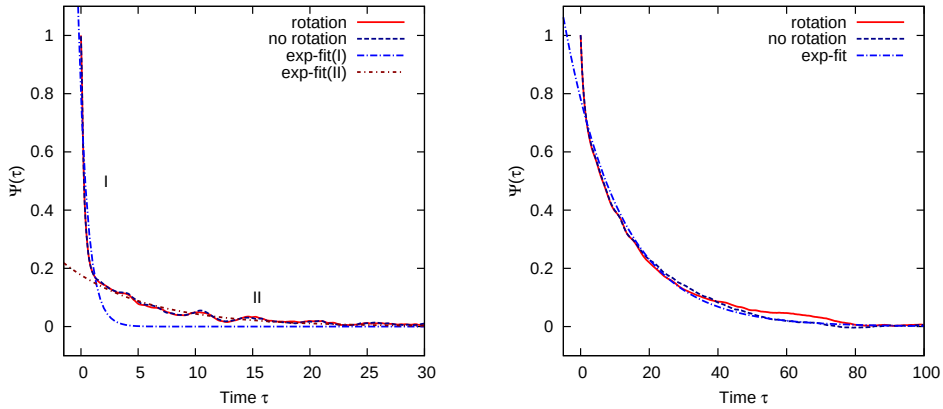

Figure 3: Velocity-autocorrelation-functions (VACF) for a light (left: $\rho_{\mathrm{RB}}/\rho_{\mathrm{f}}=1$) and a ten times heavier nanoparticle (right: $\rho_{\mathrm{RB}}/\rho_{\mathrm{f}}=10$), with and without rotational degrees of freedom. While the left VACF must be fitted by two exponentials (I and II), the right VACF shows exponential decay with one single time constant and hence Brownian behaviour. The VACFs $\Psi(t)\equiv\langle\mathbf{v}(t)\cdot\mathbf{v}\rangle$ have been normalised by $\langle\mathbf{v}\cdot\mathbf{v}\rangle=3k_BT/M$. The extension of the exponential to negative times serves only for improving the distinction of curves. The unit of time is given in Table 1.

and hence delays the $t^{-3/2}$ behaviour of the hydrodynamic tail (of region "III") to times where noise makes it unobservable. We expect a hydrodynamic tail to be detectable for $\rho_{RB}/\rho_f=1$ but this would require improved statistics for this case which is of minor interest for the work presented here. Then, for the simulations with $\rho_{RB}/\rho_f=1$ and a confinement by walls, we have to ask the question whether the change in the behaviour of the hydrodynamic tail being now proportional to $t^{-5/2}$ as theoretically predicted by Felderhof [20] can be detected. Additionally we see that the presence or exclusion of rotation does not have a major effect.

4.2 Spatially dependent diffusion constant

Fig. 4 shows the computed profiles of the anisotropic diffusion coefficients for the spherical nanoparticle and the nano-tetrahedron with properties as given in Table 2. Both nanoparticles have an equal mass density $\rho_{\mathrm{RB}}=10\,m^*/l^{*3}$ but different volume and mass due to a different number of particles (140 vs. 56) and effective radius R'. We normalize the diffusion values with the bulk diffusion D_0 and normalise the distance between particle and wall to the effective particle radius R. The bulk diffusion D_0 was calculated through the Green-Kubo integral (2.9) from simulations in a cubic box with periodic boundary conditions (PBC) and edge length $L=32\sigma$ resulting in a finite-size diffusion constant D_L^{PBC} to give

$$D_0=D_L^{\mathrm{PBC}}\left(1-\frac{R\xi}{L}\right), \tag{4.1}$$

where $\xi\approx 2.837$ is a correction factor according to [29]. In the correction given there, we have expressed the shear viscosity η in the bulk by the effective radius R and the diffusion

constant D_0 through the Stokes-Einstein relation (2.8) leading to the above expression.

The diffusion profile, that we obtain for a nano sphere (cf. Fig. 4a) is shown in Fig. 4c. The plot shows the normal and the parallel component of the nanoparticle's self diffusion coefficient as a function of the nanoparticle's distance to the planar wall. Also plotted are the inverted analytical correction terms (2.5, 2.6). We repeated the MD-simulations for the nano tetrahedron (cf. Fig. 4b). In the vicinity of the wall both objects show diffusive behaviour in good agreement with theory. For increasing distance, the parallel diffusion constant of the sphere deviates from the theoretical prediction, while the perpendicular diffusion parameter remains in good agreement.

The tetrahedron's diffusion constants are plotted against the distance to the wall normalised by the effective radius $R=2.60\sigma$. Note that there is no significant change in behaviour due to the non-spherical shape of the nanoparticle. Moreover, the tetrahedron's diffusion values agree with the theory for the equivalent sphere up to large distances.

We attribute the deviation of the third parallel diffusion constant from the wall to additional errors due to the measurement algorithm which are not accounted for by the given error-bars. These may stem from the huge number of very short trajectories that result in the region close to the wall possibly leading to a partially incomplete equipartition. We are currently unable to explain the disagreement of measurement and theory for the sphere's parallel diffusion component for $z/R>1$. An inconsistency due to different finite size effects parallel and perpendicular to the wall may give rise to this deviation.

4.3 Nanoparticle orientation

Since no significant shape dependence has been observed for the diffusion coefficient, we take a closer look at the orientation and the rotational motion of the nanosphere and nanotetrahedron when brought close to the planar wall. Therefore, we transform the trajectory of the orientation of the nanoparticle, which is given in quaternions $q(t)$, into spherical coordinates $\phi(t)$,$\theta(t)$,$r=1$ of a representative vector which is constant in the nanoparticle's local coordinate system. We define a region close to the wall, with a small gap. This gap of 0.54 nm serves to avoid artefacts in the statistics due to close contact with the wall. The parts of the trajectories lying inside this region are extracted in order to compute histograms of the spherical coordinates $\phi(t)$,$\theta(t)$. The orientational histograms for the spherical cluster and the tetrahedron are shown in Fig. 5. ϕ should be equally distributed in case of isotropy and the distribution of θ should be $\sin(\theta)$. Besides the noise, both nanoparticle shapes show an isotropic orientation near the wall, thus we do not observe any significant shape dependence.

5 Summary and discussion

Summarizing, we have presented a molecular dynamics investigation of the hydrodynamic interactions of spherical and tetrahedral nanoparticles close to planar walls.

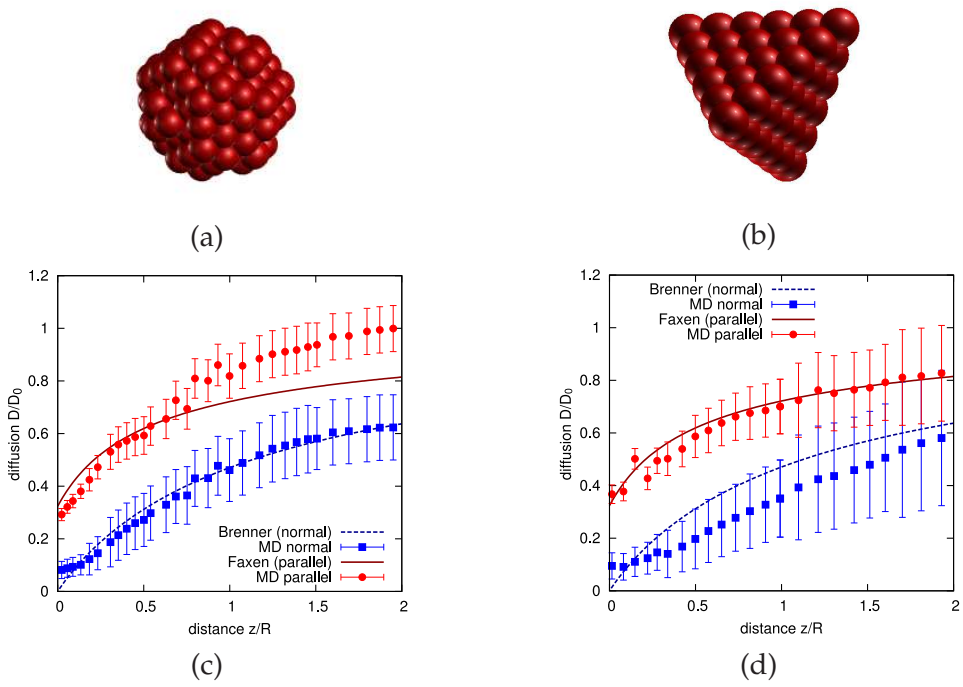

Figure 4: Top: A cluster of (a) 140 MD particles approximating a spherical nanoparticle and (b) 56 MD particles approximating a nano-tetrahedron. Bottom: Profile of the diffusion coefficient for the (c) sphere and (d) for the tetrahedron. The errors of the diffusion values increase with the distance, because of less data.

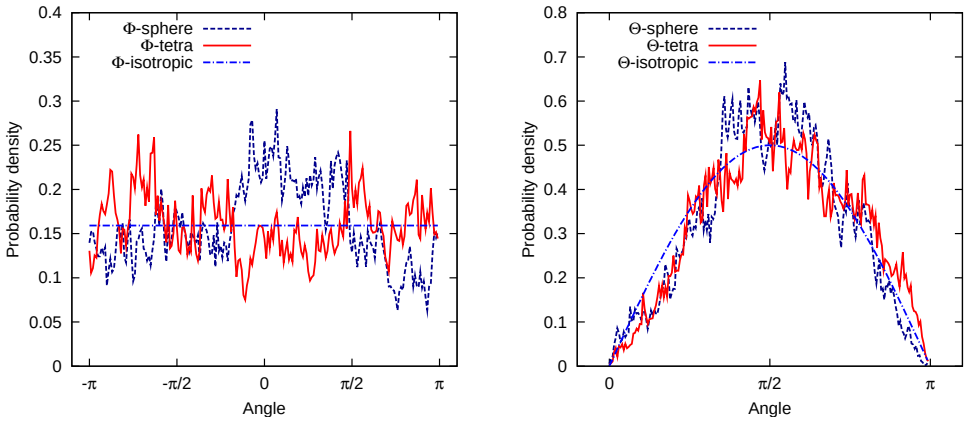

Figure 5: Histograms of the orientation angles of nano sphere and tetrahedron. The ideal isotropic distributions are plotted as well.

For both shapes, numerical data are found to reproduce the anisotropic correction to fluid viscosity, as predicted by the continuum hydrodynamic theories of Faxén and Brenner [13–15]. This is an interesting finding, because in experimental work [30,31], the parallel diffusion coefficient could either not be measured independently of the normal

one or the measured parallel diffusion coefficient showed large deviation from the theoretic predications of Faxén and Brenner for particle sizes of 100 nm. We also see, that the particle touches the wall, which was claimed to be unphysical in previous theoretical work [32]. The present results provide yet another evidence of the broad range of validity of hydrodynamic theory, down to a very few atomic distances [23], in our case down to a molecular radius σ. For the spherical nanoparticle a very good agreement is observed for the diffusion constant perpendicular to the wall. A pronounced deviation in the breakdown region near the wall is shown. On the other hand the parallel diffusion constant for a sphere follows the theoretical prediction down to the shortest distances resolved by our simulation results, where no singular behaviour of the theory is present. In contrast, at larger distances the deviations are increasing most likely due to the above mentioned inconsistency in the simplified treatment of finite size effects.

The results for the tetrahedron show very good agreement with the theory in the parallel direction, while the perpendicular direction is in good agreement within the statistical uncertainty. The deviation at short distances from the wall is pronounced in the perpendicular diffusion constant as well. This leads us to the conclusion that there is no distinct dependence due to the two different geometrical shapes of the nanoparticle used. Even though our Reynolds number tends to zero and is hence very different from Vergeles et al.'s [18], we can confirm their conclusion that hydrodynamics holds down to molecular scales. Challa and van Swol's observed solvation force's [19] did not seem to influence our results.

Only very recently, experimental setups for Brownian particles were devised, which enable to measure the normal and the parallel component of the anisotropic particle mobility independently by light scattering and the evaluation of correlation functions [33]. The MD scheme presented in this work can therefore offer a useful complement and alternative to experimental investigation.

Acknowledgments

The authors acknowledge fruitful discussions with Pep Español and Howard Stone and funding by the DFG via SFB499 and by the University of Freiburg through the German Excellence Initiative.

References

[1] G. R. Kneller and G. Sutmann K. Hinsen. Mass and size effects on the memory function of tracer particles. Journal of Chemical Physics, 118:5283–5286, 2003.
[2] A. Einstein. On the theory of brownian movement. Ann. Phys., 19:371–381, 1906.
[3] R. Zwanzig. Nonequilibrium Statistical Mechanics. Oxford University Press, Oxford, 2001.
[4] L.D. Landau and E.M. Lifschitz. Hydrodynamik. Akademie-Verlag, Berlin, 5th edition, 1971.
[5] Zhenli Zhang and Sharon C. Glotzer. Self-assembly of patchy particles. Nano Letters, 4:1407–1413, 2004.

[6] Z. Zhang, A.S. Keys, T. Chen, and S.C. Glotzer. Self-assembly of patchy particles into diamond structures through molecular mimicry. Langmuir, 21:11547–11551, 2005.
[7] S. Maenosono, C.D. Dushkin, and Y. Yamaguchi. Direct measurement of the viscous force between two spherical particles trapped in a thin wetting. Colloid & Polymer Science, 277:993–996, 1999.
[8] B. Wu, A. Ho, N. Moldovan, and H. D. Espinosa. Direct deposition and assembly of gold colloidal particles using a nanofountain probe. Langmuir, 23:9120–9123, 2007.
[9] A. Rohrbach. Observing secretory granules with a multiangle evanescent wave microscope. Biophysical Journal, 78:2641V2654, 2000.
[10] A. Rohrbach, H. Kress, and E.H.K. Stelzer. Three-dimensional tracking of small spheres in focused laser beams: influence of the detection angular aperture. Optics Letters, 28:411–413, 2003.
[11] A. Rohrbach, C. Tischer, D. Neumayer, E.L. Florin, and E.H.K. Stelzer. Trapping and tracking a local probe with a photonic force microscope. Review of Scientific Instruments, 75:2197–2210, 2004.
[12] S. C. Kohale and R. Kharea. Molecular dynamics simulation study of friction force and torque on a rough spherical particle. Journal of Chemical Physics, 132:234706–(7), 2010.
[13] H. Faxen. Der Widerstand gegen die Bewegung einer starren Kugel in einer zähen Flüssigkeit, die zwischen zwei parallelen ebenen Wänden eingeschlossen ist. Annalen der Physik, 373:89–119, 1922.
[14] Howard Brenner. The slow motion of a sphere through a viscous fluid towards a plane surface. Chemical Engineering Science, 16(3-4):242–251, 1961.
[15] J. Happel and H. Brenner. Low Reynolds number hydrodynamics. kluwer, 1983.
[16] J.W. Berenshot, N.R. Tas, H.V. Jansen, and M. Elwenspoek. Chemically anisotropic single-chrystalline silicon nanotetrahedra. Nanotechnology, 20:475302–(7), 2009.
[17] M. Elwenspoek, L. Abelmann, E. Berenschot, J. van Honschoten, H. Jansen, and N. Tas. Self-assembly of (sub-)micron particles into supermaterials. Journal of Micromechanics and Microengineering, 20:064001–(28), 2010.
[18] Maxim Vergeles, Pawel Keblinski, Joel Koplik, and Jayanth R. Banavar. Stokes drag at the molecular level. Phys. Rev. Lett., 75:232–235, Jul 1995.
[19] Sivakumar R. Challa and Frank van Swol. Molecular simulations of lubrication and solvation forces. Phys. Rev. E, 73:016306, Jan 2006.
[20] B. U. Felderhof. Effect of the wall on the velocity autocorrelation function and long-time tail of brownian motion in a viscous compressible fluid. The Journal of Chemical Physics, 123(18):184903, 2005.
[21] H. A. Lorentz. Abhandlungen über Theoretische Physik, volume 1. Teubner, Leipzig, 1907.
[22] I. Pagonabarraga, M. H. J. Hagen, C. P. Lowe, and D. Frenkel. Algebraic decay of velocity fluctuations near a wall. Phys. Rev. E, 58:7288–7295, Dec 1998.
[23] J.P. Boon and S. Yip. Molecular Hydrodynamics. Dover Puplications, Inc. New York, 1980.
[24] H.C. Anderson, D. Chandler, and J.M. Weeks. Roles of repulsive and attractive forces in liquids : The equilibrium theory of classical fluids. Adv. Chem. Phys., 34:105–156, 1976.
[25] D. C. Rapaport and E. Clementi. Eddy formation in obstructed fluid flow: A molecular-dynamics study. Phys. Rev. Lett., 57:695–698, Aug 1986.
[26] Jürgen Horbach and Sauro Succi. Lattice Boltzmann versus molecular dynamics simulation of nanoscale hydrodynamic flows. Phys. Rev. Lett., 96:224503, Jun 2006.
[27] I.P. Omelyan. On the numerical integration of motion for rigid polyatomics: The modified quaternion approach. Computers in Physics, 12(1):97–103, Jan/Feb 1998.

[28] Thomas Franosch, Matthias Grimm, Maxim Belushkin, Flavio M. Mor, Giuseppe Foffi, Laszlo Forro, and Sylvia Jeney. Resonances arising from hydrodynamic memory in brownian motion. Nature, 478(7367):85–88, 2011.
[29] I. C. Yeh and G. Hummer. System-size dependence of diffusion coefficients and viscosities from molecular dynamics simulations with periodic boundary conditions. J. Phys. Chem. B, 108:15873–15879, 2004.
[30] N. Ostrowsky and N. Garnier. Quasi-elastic light-scattering from an evanescent wave to probe particle wall interactions. Biochemical Society Transactions, 19:500–501, 1991.
[31] K.D. Kihm, A. Banerjee, C.K. Choi, and T. Takagi. Near-wall hindered brownian diffusion of nanoparticles examined by three-dimensional ratiometric total internal reflection fluorescence microscopy (3-d r-tirfm). Experiments in Fluids, 37:811–824, 2004.
[32] A.J. Goldman, R.G. Cox, and H. Brenner. Slow viscous motion of a sphere parallel to a plane wall. I. Motion through a quiescent fluid. Chemical Engineering Science, 22:637–651, 1967.
[33] P. Holmqvist, J.K.G. Dhont, and P.R. Lang. Anisotropy of brownian motion caused only by hydrodynamic interaction with a wall. Physical Review E, 74:021402–(5), 2006.